ACS Photonics

pubs.acs.org/journal/apchd5

Article

Gate-Tunable Transmissive Metasurfaces with Dual-Resonance-Enhanced Modulation

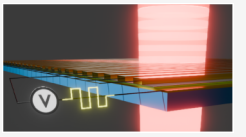
Sota Ito, Soh Uenoyama,* Ruzan Sokhoyan, Jared Sisler, and Harry A. Atwater*

Cite This: *ACS Photonics* 2026, 13, 3742−3749

Read Online

ACCESS | Metrics & More | Article Recommendations | Supporting Information

ABSTRACT: Electrically tunable metasurfaces enable dynamic control of light in ultrathin optical platforms. Most solid-state implementations rely on reflection-mode operation to achieve strong light−matter interaction, which limits their compatibility with transmissive and monolithically integrated photonic systems. In this work, we demonstrate a solid-state, electrically tunable transmissive metasurface based on a metal−oxide−semiconductor (MOS) architecture that overcomes this constraint by engineering vertical optical confinement in transmission mode. The metasurface consists of plasmonic gold nanoantennas separated from a semitransparent gold layer by an Al_2O_3/indium tin oxide (ITO) stack, with an additional amorphous silicon layer beneath the semitransparent metal. This vertical heterostructure forms a Fabry−Pérot cavity that couples to a gap plasmon resonance supported by the nanoantennas, enabling strong electric-field confinement within the electrically gated ITO accumulation layer while preserving forward transmission. Electrical bias drives the ITO into the epsilon-near-zero regime, producing a pronounced modulation of the transmitted intensity. The device experimentally exhibits a peak transmittance of 24.4% and a relative transmission modulation of 9.4% at a wavelength of 1494 nm under a low driving voltage of under ±3.5 V bias, in good agreement with numerical simulations. High-speed measurements reveal a −3 dB modulation bandwidth of 7.7 MHz, primarily limited by device capacitance. The fully solid-state, CMOS-compatible architecture provides a compact platform for high-speed transmissive optical modulation, with potential applications in beam steering and free-space optical communications.



KEYWORDS: *Gate-tunable metasurface, Active transmissive metasurface, Free-space transmissive amplitude modulator, Epsilon-near-zero (ENZ) metasurface, Indium tin oxide (ITO), Plasmonic metasurface, Gap plasmon resonance*

1. INTRODUCTION

A metasurface is an ultrathin, two-dimensional array of subwavelength resonators that can precisely control the wavefront of the reflected or transmitted light by tailoring the scattering properties of each subwavelength resonator. This capability has enabled a wide range of static optical functionalities, including metalenses,[1−5] holography,[6−9] and optical vortex beam generation.[10] However, because the optical response of the nanostructures is intrinsically linked to their physical geometry and material composition, the functionality of a conventional metasurface is fixed after fabrication, preventing dynamic control or reconfigurability.

Recently, tunable metasurfaces have emerged as a promising route to overcome the static limitations of conventional metasurfaces and broaden their range of functionalities.[11] Dynamic control of optical responses is particularly valuable for applications such as light detection and ranging (LiDAR),[12] free-space optical communication (FSO),[13] and optical limiting,[14] which demand high-speed modulation and precise wavefront control. Among various strategies for tunability, solid-state implementations of active metasurfaces offer important advantages, including mechanical robustness, compact form factors, and compatibility with integrated photonic platforms. When implemented on a solid-state platform, tunable metasurfaces offer enhanced robustness and integration potential, making them particularly appealing for next-generation photonic systems.

However, most experimentally demonstrated active metasurfaces to date operate in reflection mode.[15−21] In reflective configurations, the nanoantennas can be placed above a metallic back reflector with a spacer layer, enabling strong electric field confinement within nanoscale gaps where the tunable material is incorporated. This strategy has facilitated versatile wavefront manipulation, but it also introduces inherent constraints associated with reflective operation. Specifically, reflective metasurfaces require illumination from an external, off-chip light source, which increases the overall form factor and limits system-level integration. In contrast, transmissive metasurfaces offer greater compatibility with chip-scale light sources, such as photonic crystal surface-emitting lasers (PCSELs)[22] and vertical-cavity surface-emitting lasers (VCSELs),[23] and thus provide a more promising route toward compact and fully integrated photonic platforms.

Received: March 10, 2026
Revised: June 1, 2026
Accepted: June 2, 2026
Published: June 12, 2026



Downloaded from pubs.acs.org/apchd5/article-pdf/13/13/3742/6529140/acsphotonics.6c00577.pdf by CALIFORNIA INST OF TECHNOLOGY, Ruzan Sokhoyan on 27 August 2026

© 2026 American Chemical Society

https://doi.org/10.1021/acsphotonics.6c00577
ACS Photonics 2026, 13, 3742−3749

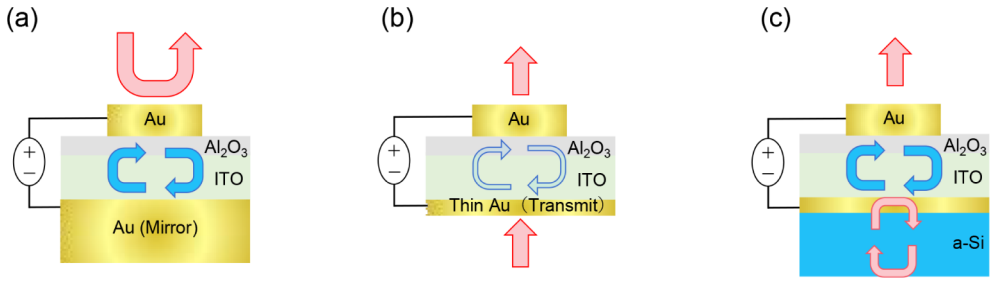


Figure 1. Concept of the transmissive tunable metasurface. (a) General configuration for a reflective tunable metasurface. (b) Transmissive metasurface with a reduced-thickness semitransparent metal bottom layer. (c) An a-Si layer is placed beneath the semitransparent Au layer to achieve high transmittance.

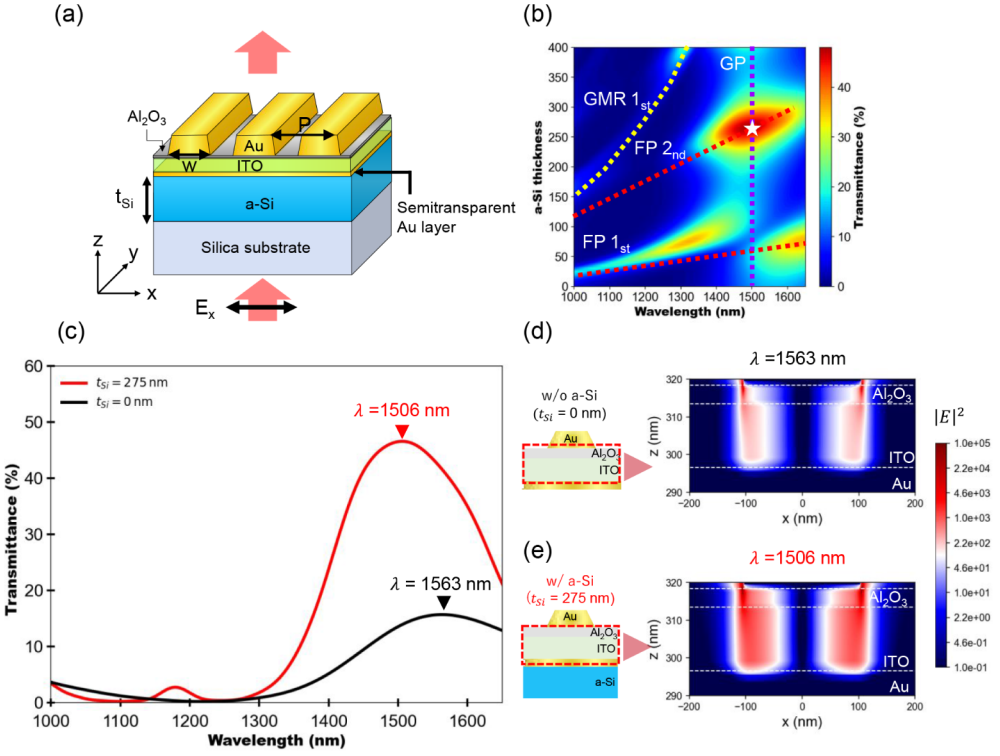


Figure 2. Design and simulation results of the transmission-tunable metasurface (a) Schematic of the proposed tunable metasurface. Each Au nanoantenna is modeled as an infinitely long stripe with a thickness of 70 nm and a width of W = 210 nm. The period of the metasurface is P = 400 nm. (b) Full wave simulation results: transmission map as a function of incident wavelength and a-Si thickness. The yellow, red, and purple dashed lines indicate the first GMR, the first and second FP modes, and the GP mode. (c) Transmittance spectra with (red solid line, t_{Si} = 275 nm) and without (black solid line) the a-Si layer. (d, e) Near-field electric-field intensity distributions of the metasurface without and with the a-Si layer at wavelengths of 1506 and 1563 nm, respectively. The schematics indicate the x−z cross-sectional view, where the near-field is monitored within the Al_2O_3/ITO region of the Au nanoantenna/Al_2O_3/ITO/Au multilayer structure, as highlighted by the red boxes.

Recently, several research groups have demonstrated tunable transmissive metasurfaces;[24−32] however, many of these approaches rely on slow mechanisms such as ionic transport,[24] liquid-crystal molecules,[25−27] metallic polymers,[28] or MEMS-based mirror structures.[29,30] These mechanisms inherently limit the modulation speed and, in the case of mechanical actuation, can introduce reliability and stability challenges.

Among solid-state platforms, electro-optic (EO) polymers[31,32] and lithium niobate (LN)[33−35] have demonstrated high-speed modulation without mechanical actuation. However, the refractive index change in these materials is relatively small—on the order of 10^{-3}—which typically necessitates integration with high-Q resonant structures to enhance light−matter interaction. While such resonant enhancement improves modulation efficiency, it also leads to narrow optical bandwidth and increased sensitivity to fabrication imperfections, ultimately limiting the robustness of EO metasurfaces. In addition, the incorporation of EO materials typically demands custom fabrication processes that are not fully compatible with standard CMOS technology, posing further challenges for large-scale integration and mass production.

Indium tin oxide (ITO)-based tunable metasurfaces[15] offer a promising alternative since they enable fast response times, dense integration, and CMOS compatibility. A representative type is the metal−oxide−semiconductor (MOS) configuration,[15−21] consisting of a metal nanograting, an insulating layer (e.g., HfO_2 or Al_2O_3), and a semiconductor layer (e.g., ITO) stacked on a metallic mirror (Figure 1a). In this configuration, vertical biasing between the nanograting and the bottom mirror enables carrier accumulation in the semiconductor

https://doi.org/10.1021/acsphotonics.6c00577
ACS Photonics 2026, 13, 3742−3749

Downloaded from pubs.acs.org/apchd5/article-pdf/13/13/3742/6529140/acsphotonics.6c00577.pdf by CALIFORNIA INST OF TECHNOLOGY, Ruzan Sokhoyan on 27 August 2026

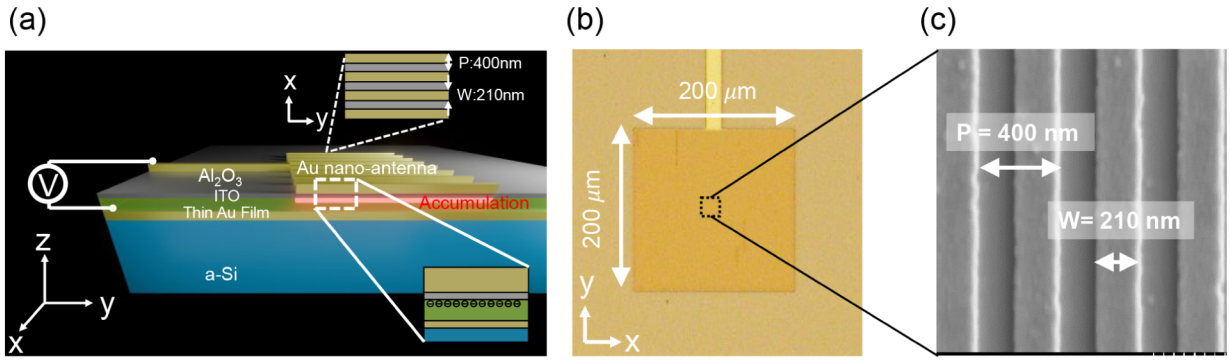


Figure 3. Fabrication results of the tunable metasurface. (a) Schematic of the voltage-biasing configuration for the transmissive tunable metasurface, consisting of an Au nanoantenna/Al_2O_3/ITO/semitransparent thin Au layer/a-Si stack on a silica substrate. (b) Optical microscope image of the fabricated Au nanoantenna array with an overall size of 200 μm × 200 μm. (c) Magnified scanning electron microscopy (SEM) image of the Au nanoantenna array, showing a period of 400 nm and an antenna width (w) of 210 nm.

layer, which is located in the tight gap between the metallic mirror and the top antenna. The accumulated carriers drive the thin ITO layer into the epsilon-near-zero (ENZ) regime, where strong electric-field enhancement occurs and produces a pronounced change in the optical response. This ENZ-assisted modulation mechanism enables ultrafast electrical control of optical amplitude,[15] phase,[16−19] polarization,[20] and even frequency,[21] all without any moving components.

Several previous works have investigated ITO-based dynamically tunable transmissive metasurfaces.[36−39] Thomaschewski et al. presented a transmission-tunable metasurface by hybridizing a plasmonic Au grating with an ITO layer.[37] However, this approach makes it difficult to tightly confine the incident light in the ITO layer, which is located underneath the metal grating. As a result, this work reports only modest transmittance modulation. Lee et al. recently demonstrated a transmissive modulator based on a hybrid plasmonic waveguide mode; however, the reported 3 dB bandwidth of 826 kHz was found to be limited by the electrical RC time constant extracted from their device capacitance and ITO resistance.[38] Prior theoretical work has also proposed all-dielectric transmissive metasurfaces that hybridize an ITO accumulation layer with Si nanodisks; however, these designs exhibit inherently low transmission efficiencies—on the order of only a fraction of a percent—because the strongly confined dielectric resonances of the Si nanoantennas couple only weakly into the forward-propagating channel.[39]

Here, we design and experimentally demonstrate ITO-based active plasmonic transmissive metasurfaces, which exhibit both a relatively high transmittance of 25% and a high 3 dB modulation frequency of 7.7 MHz. Our metasurface design relies on the coupling of the gap plasmon (GP) and Fabry−Perot (FP) resonant modes to achieve two seemingly conflicting properties—high transmittance and tight confinement of the electric field in the ITO layer. Under applied electrical bias, we experimentally observe a relative transmittance modulation of 9.4%. Our electrically tunable metasurface can be readily integrated with chip-scale light sources such as PCSELs and VCSELs.

2. RESULTS AND DISCUSSION

2.1. Design of the Transmissive Tunable Metasurface

In our design effort, we begin with a previously reported reflective GP metasurface (Figure 1a) and reduce the thickness of its metal back mirror (Figure 1b), thereby converting it into a semitransparent layer that enables transmission-mode operation. However, this simple approach results in modest transmittance and limited transmittance modulation. To enhance our metasurface performance, we introduce an additional FP cavity underneath the semitransparent Au layer and couple the FP mode to the GP mode, which is confined between the Au antenna and the bottom semitransparent Au layer (Figure 1c). This enables tight confinement of the incident light within the dielectric gap region while maintaining high transmittance, as illustrated in Figure 1c.

The proposed metasurface design is summarized in Figure 2a. The metasurface element consists of a 70 nm-thick Au nanoantenna, a 5 nm-thick insulating Al_2O_3 layer, a 17 nm-thick ITO layer, a 20 nm-thick semitransparent Au layer, and an amorphous silicon (a-Si) layer deposited on a silica substrate (Figure 2a). The period (P) and width (W) of the Au nanoantenna are P = 400 nm and W = 210 nm, respectively. In the simulated structures, the Au nanoantenna has a tapered sidewall (~70° from vertical), consistent with the fabrication results obtained under the same conditions.[40] This tapered profile originates from shadowing effects during metal evaporation, where Au deposited on the resist sidewalls partially acts as a secondary mask, effectively narrowing the antenna opening. In our simulations, the metasurface is illuminated from within the SiO_2 substrate, and the impinging plane wave is linearly polarized along the x-direction.

Figure 2b maps the metasurface transmittance as a function of the wavelength of the incident light (λ = 1000−1650 nm) and the thickness of the a-Si layer (150−400 nm). The full thickness range of the a-Si layer (0−800 nm) is shown in Supporting Information S1, Figure S1a. The resonant wavelength of the second-order FP mode (red dotted line) exhibits an approximately linear dependence on the a-Si thickness, whereas the spectral position of the GP mode (purple dotted line) is primarily defined by the width of the Au nanoantenna (W = 210 nm). We note that the FP modes can be identified in the transmittance spectrum of the planar heterostructure beneath the Au stripes (Figure 2a) when the Au stripe antennas are removed (see Supporting Information S2, Figure S2).

Achieving high transmittance and strong light confinement requires significant overlap between FP and GP modes, which can be achieved by carefully choosing the thickness of the a-Si layer and the width of the Au nanoantenna. As seen in Figure 2b, at wavelengths around 1500 nm, we achieve a high

https://doi.org/10.1021/acsphotonics.6c00577
ACS Photonics 2026, 13, 3742−3749

Downloaded from pubs.acs.org/apchd5/article-pdf/13/13742/6529140/acsphotonics.6c00577.pdf by CALIFORNIA INST OF TECHNOLOGY, Ruzan Sokhoyan on 27 August 2026

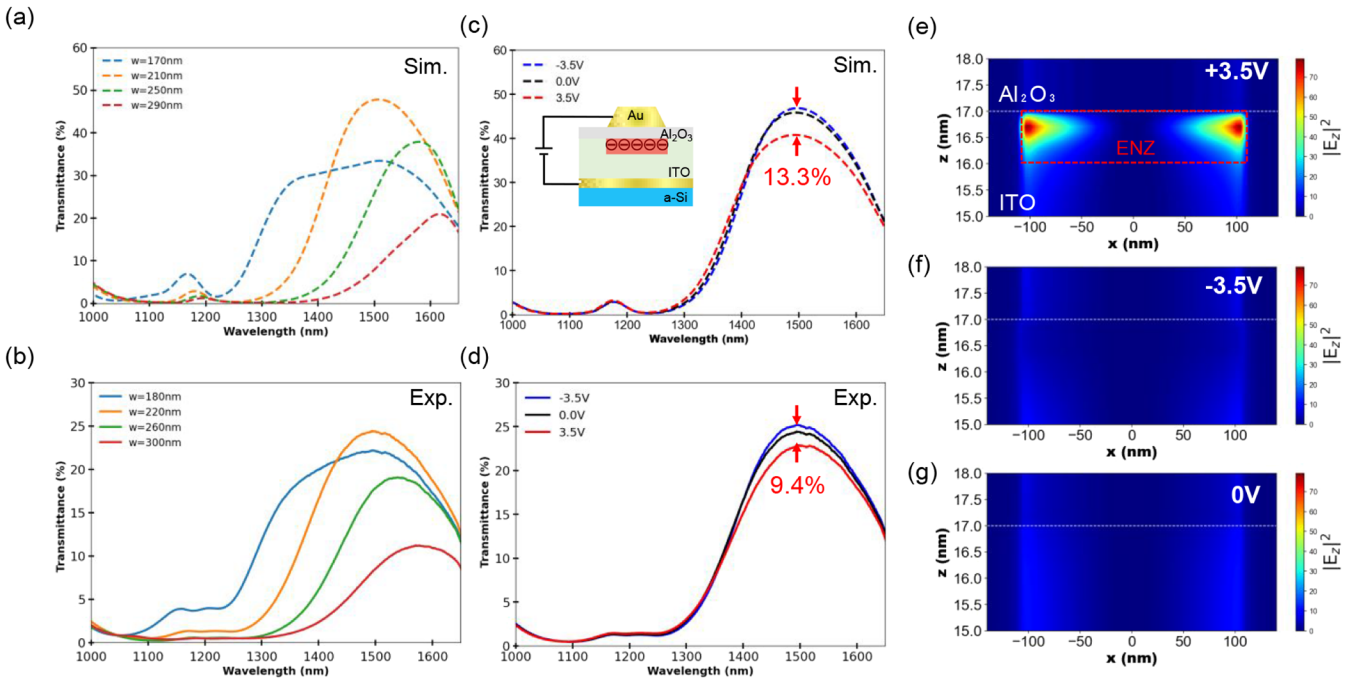


Figure 4. Transmission spectra and near-field electric intensity maps (a, b) Simulated and experimental transmission spectra, respectively. The blue, orange, green, and red lines correspond to widths W = 170, 210, 250, and 290 nm, respectively. (c, d) Simulated and experimental transmission modulation as a function of incident wavelength, respectively. The red, blue, and black dotted lines correspond to applied voltages of +3.5 V, −3.5 V, and 0 V, respectively. (e, f, g) Near-field electric intensity distributions between the Al_2O_3 and ITO layers for +3.5 V, −3.5 V, and 0 V, respectively. The red dotted region in (e) indicates the ENZ region.

transmittance of 50% when the thickness of the a-Si layer is taken as 275 nm. Figure 2c shows the transmittance spectra with and without the a-Si layer, corresponding to the a-Si thicknesses of t_{Si} = 275 nm and t_{Si} = 0 nm. An additional transmission peak at 1170 nm originates from the guided-mode resonance (GMR) supported by the Si slab (see Supporting Information S3 for details). As seen in Figure 2c, the presence of the a-Si layer enhances the transmittance compared to the case without it. Figure 2d and e show the near-field electric field intensity distributions within the dielectric gap between the Au nanoantennas and the semitransparent Au layer, without and with the a-Si layer, respectively. Note that the transmission peak wavelengths differ depending on the presence of the a-Si layer. Therefore, for a fair comparison, the field distributions are evaluated at respective wavelengths corresponding to the maximum transmittance (1563 and 1506 nm). As shown in Figure 2d and e, light is strongly confined within the dielectric region between the Au nanoantennas and the semitransparent Au layer when the a-Si layer is present (for additional electric field profiles, see Supporting Information S4). This enhanced confinement arises due to the coupling of the gap plasmon and Fabry−Pérot modes.

2.2. Fabrication Results

Next, we fabricate the designed metasurface and investigate its electrically tunable optical performance. A bias voltage is applied between the nanoantenna array and the semitransparent Au layer, inducing transmittance changes by forming an accumulation layer in the ITO (for schematic, see Figure 3a). Figure 3b shows the optical microscopy image of the fabricated metasurface. The size of the metasurface array is 200 μm × 200 μm. The magnified scanning electron microscopy (SEM) image of the Au nanoantennas is shown in Figure 3c. Thus, the fabricated Au nanoantennas are approximately 200 μm-long and are arranged periodically along one direction with a period of 400 nm, forming a one-dimensional array. The fabricated Au nanoantenna exhibits a pitch of 400 nm and an arm width of 210 nm, consistent with the design parameters.

2.3. Transmission Results under Applied Voltage

Next, we investigate the dependence of the metasurface transmittance spectrum on the width of the top Au nanoantennas. Figure 4a and b present the simulated and measured transmittance spectra, respectively, as functions of the incident wavelength (λ = 1000−1650 nm) for different nanoantenna widths (W = 170, 210, 250, and 290 nm). Both the simulation and experiment show that increasing the nanoantenna width shifts the transmission peak toward longer wavelengths. This behavior can be attributed to the antenna resonance condition, whereby the resonance wavelength increases approximately proportionally with the nanoantenna width in a fixed dielectric environment (15). Notably, when W = 210 nm, which corresponds to the FP resonance condition, the transmission peak appears near 1494 nm. Under this condition, the experiment yields a maximum transmission of 24.4%, where the GP and FP resonances overlap. These results demonstrate good agreement with the simulated trend, although the absolute transmission values are lower in the experiment. This discrepancy likely arises from over-deposition of the Au semitransparent layer, resulting in a thickness exceeding the intended design value (see Supporting Information S5).

Figure 4c and d show the relative transmission modulation as a function of wavelength for the simulated and measured results, respectively. In our work, the maximum applied voltage between the Au antennas and the ITO layer is ±3.5 V,

https://doi.org/10.1021/acsphotonics.6c00577
ACS Photonics 2026, 13, 3742−3749

Downloaded from pubs.acs.org/apchd5/article-pdf/13/13742/6529140/acsphotonics.6c00577.pdf by CALIFORNIA INST OF TECHNOLOGY, Ruzan Sokhoyan on 27 August 2026

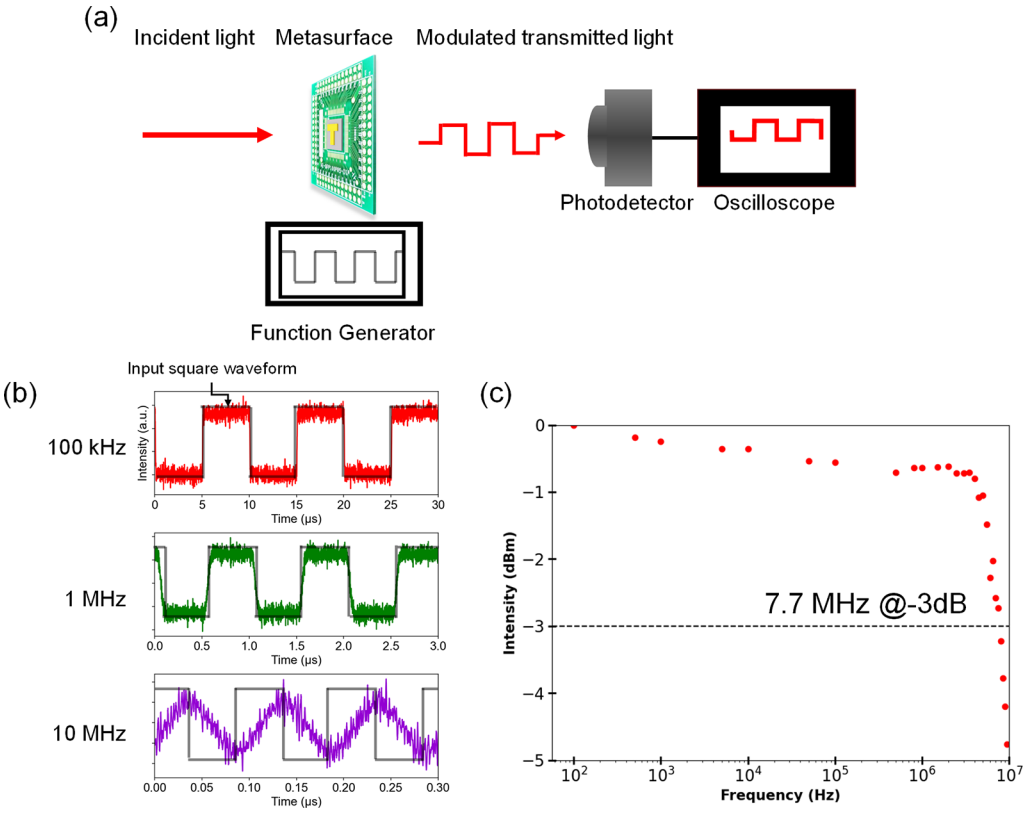


Figure 5. High-speed modulation characteristics of the metasurface. (a) Schematic illustration of the high-speed measurement concept. A collimated optical beam is incident on the metasurface, whose transmission is modulated by an applied square-wave electrical bias (gray waveform). The temporally modulated transmitted signal is detected by a photodetector and sent to an oscilloscope for analysis. The waveforms are shown for illustration purposes only and are not to scale. (b) Transmission intensity as a function of modulation time. The gray line schematically represents the input square-wave modulation signal, while the red, green, and purple lines correspond to the modulated transmission at 100 kHz, 1 MHz, and 10 MHz, respectively. (c) Transmitted intensity as a function of modulation frequency. The black dashed line indicates the −3 dB threshold.

corresponding to an electric field of 0.7 V/nm across the 5 nm-thick Al_2O_3 dielectric layer. The relative transmission modulation is defined as (T(V = +3.5 V) − T (V = 3.5 V)/ T (V = −3.5 V). In the simulation, a maximum relative transmission modulation of 13.3% is observed between applied voltages of −3.5 V and +3.5 V at a wavelength of 1494 nm. The experimental measurements exhibit a relative transmission modulation of 9.4%, demonstrating good agreement with the simulated trend.

When a positive bias (V = +3.5 V) is applied between the Au nanoantenna and the semitransparent Au layer, the carrier concentration in the ITO at the Al_2O_3/ITO interface increases significantly, forming a thin electron accumulation layer with a thickness of a few nanometers. As a result, the permittivity of the ITO approaches the epsilon-near-zero (ENZ) regime (see Supporting Information, S6), leading to strong electric-field confinement within the ENZ region at λ = 1494 nm (Figure 4e). This ENZ mode is known to induce pronounced changes in the optical response of nanophotonic structures.[37,38] Consequently, the strongly confined electric field enhances optical absorption in the ENZ region, resulting in reduced transmittance.

In contrast, when a negative bias (V = −3.5 V) is applied, a carrier depletion layer forms at the Al_2O_3/ITO interface. Under this condition, the strong electric-field confinement observed under positive bias is absent, and the field distribution at λ = 1494 nm is weakened and partially delocalized, as shown in Figure 4f. Moreover, the electric-field distributions at V = 0 V (Figure 4g) and −3.5 V (Figure 4f) are similar, indicating that transmittance modulation under negative bias is minimal compared to that under positive bias.

Notably, in terms of optical efficiency, the transmissive tunable metasurface demonstrated here exhibits a significantly higher transmission (24.4% in this experiment) than conventional metal−insulator−metal (MIM) reflection-type metasurfaces (∼5%).[19] However, due to the intrinsic limitations of two-port systems, transmissive metasurfaces generally do not achieve phase modulation efficiencies comparable to those of reflection-type metasurfaces.[41]

While the present device does not target complete extinction in the off state, full suppression of transmission could, in principle, be achieved through alternative design choices, albeit at the expense of reduced on-state transmittance. In this work, we instead prioritized high transmission efficiency and high-speed modulation. From an application perspective, achieving complete suppression of transmission would further enhance the utility of the device, for example, as a high-speed optical shutter integrated above a photodetector.

2.4. Transmission Modulation under Electrical Bias

We characterized the temporal modulation performance of the metasurface by measuring its frequency response using the optical setup shown in Figure 5a, with additional experimental details provided in Methods, Section 5.2 Figure 5b shows the transmitted optical intensity as a function of time together with the applied trigger signal (blue). A square-wave voltage with a peak-to-peak amplitude of 5 V (±2.5 V) was generated using a

https://doi.org/10.1021/acsphotonics.6c00577
ACS Photonics 2026, 13, 3742−3749

Downloaded from pubs.acs.org/apchd5/article-pdf/13/13/3742/6529140/acsphotonics.6c00577.pdf by CALIFORNIA INST OF TECHNOLOGY, Ruzan Sokhoyan on 27 August 2026

function generator, and the modulation frequency was swept from 100 Hz to 10 MHz. Representative responses at 100 kHz (red), 1 MHz (green), and 10 MHz (purple) are shown in Figure 5b.

At 100 kHz, the transmitted intensity closely follows the input signal with no observable phase delay. At 1 MHz, a slight phase lag appears between the input and transmitted signals (see Supporting Information). At 10 MHz, the transmitted signal no longer follows the input modulation, indicating a significant reduction in modulation depth.

Figure 5c plots the transmitted intensity as a function of modulation frequency. The modulation intensity is normalized to the value measured at 100 Hz. The cutoff frequency is defined as the frequency at which the transmission drops by −3 dB, as indicated by the black dashed line in Figure 5c. From this analysis, the metasurface exhibits a cutoff frequency of 7.7 MHz.

This modulation speed is primarily limited by the device capacitance, which in this experiment is determined by the array area (200 μm × 200 μm). Using the experimentally deposited insulator thickness (d = 5 nm) and the dielectric permittivity of Al_2O_3 (ε(dc) = 9), the capacitance of a 400 nm × 400 nm unit cell is estimated as $C = \varepsilon_0 \varepsilon_{dc} S/d$ yielding a value of approximately 2.6 fF. Since the total capacitance scales linearly with device area, the capacitance of a single unit cell is smaller by a factor of $(0.4\ \mu m/200\ \mu m)^2 \approx 4 \times 10^{-6}$. Accordingly, the RC time constant of an individual pixel is expected to decrease proportionally, suggesting that the modulation frequency could, in principle, reach the gigahertz range under ideal conditions. This scaling behavior highlights the strong potential of the proposed MOS-type tunable metasurface for high-speed, pixel-level modulation in compact optoelectronic systems.

3. CONCLUSIONS

In summary, we proposed a gate-tunable transmissive metasurface with a fully solid-state configuration. By precisely designing the geometry to combine FP and GP resonances, we achieved both a high transmittance of 24.4% and strong confinement of the incident light within the dielectric gap region between the semitransparent Au layer and the Au antenna. As a result, we experimentally demonstrated a 9.4% transmission modulation at a wavelength of 1494 nm with a low bias voltage of under ±3.5 V bias, which is in good agreement with simulation results. The metasurface also exhibits a high-speed response of 7.7 MHz. Our results pave the way for monolithic solid-state beam steering and advanced light-modulation devices.

4. LIMITATIONS AND FUTURE WORK

Although the proposed device demonstrates substantial modulation, further improvements in extinction ratio and optical efficiency would expand its practical applicability. While a large relative modulation can be achieved when switching between two low-transmission states, such behavior does not translate into high-performance operation if the baseline efficiency is already strongly suppressed. In ITO-based metasurfaces, this limitation stems from the intrinsic absorption of ITO, which reduces transmission even in the unbiased condition. The situation is further constrained by the fact that the tunability arises from an ultrathin (∼1 nm) carrier-accumulation layer, confining the active modulation to a very small volume. When driven into the ENZ regime, this carrier accumulation layer can exhibit enhanced absorption,[42] further diminishing efficiency. Consequently, although substantial extinction ratios may be achievable, transitions between near-unity and near-zero transmittance remain unlikely when using ITO as an active material. Integrating ITO with high-Q resonant structures offers a promising pathway, as strong field confinement and narrow line widths can amplify the effective tunability and enable switching from a finite transmission level toward near-zero transmission. Nevertheless, residual absorption in the unbiased state will continue to limit overall efficiency, highlighting the fundamental tradeoff between modulation strength and optical loss in such platforms.

In addition to ITO, other transparent conducting oxides (TCOs), such as indium zinc oxide (IZO), aluminum-doped zinc oxide (AZO), and cadmium oxide (CdO), can serve as active materials in transmissive metasurfaces. Among these, CdO is particularly promising due to its lower optical losses and smaller effective electron mass, which enable higher optical efficiency and enhanced electrically induced permittivity modulation.[42] However, its toxicity and design constraints associated with the confinement of refractive index modulation to ultrathin (∼1 nm) layers remain challenges. Both ITO and CdO are compatible with CMOS fabrication processes, although CdO has not yet been widely demonstrated in dynamically tunable nanophotonic structures.

Alternative approaches based on electro-optic (Pockels) materials, such as lithium niobate and electro-optic polymers, offer ultrafast modulation speeds reaching the GHz regime and negligible optical loss over broad wavelength ranges, but are limited by relatively small refractive index changes ($\sim 10^{-3}$).[35,36] Moreover, while LN is not intrinsically CMOS-compatible, it can be heterogeneously integrated in thin-film lithium niobate on insulator (LNOI) platforms for chip-scale implementations. In contrast, liquid-crystal-based metasurfaces[26,27] provide large index modulation (∼0.2) through molecular reorientation, albeit with significantly slower response times typically in the ∼10 Hz to 1 kHz range. Moreover, liquid-crystal-based metasurfaces are generally not CMOS-compatible due to their reliance on fluidic encapsulation and alignment layers requiring postfabrication assembly. These platforms collectively highlight the fundamental tradeoffs between modulation strength, speed, optical loss, and integration constraints in electrically tunable metasurfaces.

5. MATERIALS AND METHODS

5.1. Transmissive Modulation Measurement

A halogen lamp (PIX-UHX, NPI) was used to illuminate the metasurface through a collimating lens. A pair of 20× objective lenses (M Plan NIR 20x, NA = 0.4, Mitsutoyo) were placed face-to-face to focus and collect the transmitted light through the metasurface. The transmitted light was then split into two paths using a beam splitter. One path was directed to an NIR camera (C14041-10U, Hamamatsu) for imaging via a tube lens (f = 200 mm). The other path was directed to a spectrometer (NIRQuest+1.7, Ocean Optics). The spectrometer was configured with an exposure time of 50 ms and 10 accumulations. The transmission modulation of the metasurface was tuned by applying a DC voltage ranging from −3.5 V to +3.5 V using a function generator (WF1973, NF Corporation).

5.2. High-Speed Modulation Measurement

A tunable laser (C-band, TSL-570, Santec) was collimated using an objective lens (M Plan NIR 10×, NA = 0.26, Mitsutoyo) and a pair of

Downloaded from pubs.acs.org/apchd5/article-pdf/13/13742/6529140/acsphotonics.6c00577.pdf by CALIFORNIA INST OF TECHNOLOGY, Ruzan Sokhoyan on 27 August 2026

https://doi.org/10.1021/acsphotonics.6c00577
ACS Photonics 2026, 13, 3742−3749

mirrors, and subsequently focused onto the metasurface with another objective lens (M Plan NIR 20×, NA = 0.4, Mitsutoyo). The transmitted light passing through the metasurface was collected by another objective lens (M Plan NIR 20×, NA = 0.4, Mitsutoyo), then detected by a photodetector (PDA015C/M, Thorlabs) using an objective lens (M Plan NIR 10×, NA = 0.26, Mitsutoyo). The detected signal was sent to an oscilloscope (64MXs-B, LeCroy) for data analysis. During the measurement, a voltage was applied to the metasurface. The modulation speed was tuned using an AC voltage (Vp−p = 5.0 V, ranging from −2.5 V to +2.5 V, square wave) in the frequency range of 100 Hz to 10 MHz.

5.3. Fabrication Procedure

The metasurface was fabricated using standard nanofabrication processes, including thin film deposition, lithography, and liftoff. First, an a-Si layer with a thickness of 275 nm was deposited onto a 10 mm × 10 mm silica substrate using electron cyclotron resonance (ECR) sputtering (AFTEX-6000, JSW-AFTY). A semitransparent Au film (t = 20 nm) was then deposited on top of the a-Si layer via thermal evaporation. Subsequently, an ITO layer (t = 17 nm) was deposited by ECR sputtering. The carrier concentration and mobility of the ITO layer were controlled by adjusting the oxygen flow rate during deposition. We have observed that the optical and electrical properties of ITO films vary with film thickness. In particular, at a thickness of 17 nm, we reproducibly obtain smooth, continuous films with relatively high electron mobility. A thin Al_2O_3 insulating layer (t = 5 nm) was deposited using an atomic layer deposition (ALD) system (Fiji G2, Veeco).

Next, an electron-beam (EB) resist (ZEP 530A-6, ZEON) was spin-coated onto the sample, and the nanograting patterns were defined using electron-beam lithography (EBL) with a beam current of 400 pA and an accelerating voltage of 100 keV. The resist was developed in ZED-N60 (ZEON) for 2 min, followed by a postbake at 110 °C for 2 min. Finally, the Au nanoantenna structures were formed by a lift-off process using Remover 1165.

5.4. Simulation Conditions

Optical simulations were conducted using the finite-difference time-domain (FDTD) method with commercial software (Lumerical FDTD Solutions, Ansys). All simulation models were two-dimensional (x−z plane). Periodic boundary conditions were applied along the x-axis, and perfectly matched layers (PML) were set along the z-axis. The simulation domain ranged from −200 to 200 nm in the x-direction and −1300 to 1500 nm in the z-direction. A plane wave source under transverse magnetic (TM) polarization was placed at z = −1000 nm and illuminated along the positive z-direction. Note that the plane wave source was located within the SiO_2 substrate, which was extended into the PML boundary. A transmission monitor was positioned at z = +1200 nm. The refractive index of ITO was modulated according to the applied voltage, which was calculated using device simulations performed with commercial software (Device Lumerical, Ansys).

■ ASSOCIATED CONTENT

Supporting Information

The Supporting Information is available free of charge at https://pubs.acs.org/doi/10.1021/acsphotonics.6c00577.

S1: transmission map of the full a-Si thickness (t = 0−800 nm); S2: transmittance spectra with and without the nanoantenna; S3: dependence of the transmission spectra on the metasurface period; S4: simulated electric-field intensity distribution with and without the a-Si layer; S5: transmittance; S6: permittivity (real and imaginary parts) of ITO with and without biasing; S7: experimental setup; S8: simulation model (for CHARGE simulations) (PDF)

■ AUTHOR INFORMATION

Corresponding Authors

Soh Uenoyama − *Central Research Laboratory, Hamamatsu Photonics K.K., Hamamatsu 434-8601, Japan;* orcid.org/0000-0003-2502-5186; Email: so.uenoyama@crl.hpk.co.jp

Harry A. Atwater − *Thomas J. Watson Laboratories of Applied Physics, California Institute of Technology, Pasadena, California 91125, United States;* orcid.org/0000-0001-9435-0201; Email: haa@caltech.edu

Authors

Sota Ito − *Central Research Laboratory, Hamamatsu Photonics K.K., Hamamatsu 434-8601, Japan*

Ruzan Sokhoyan − *Thomas J. Watson Laboratories of Applied Physics, California Institute of Technology, Pasadena, California 91125, United States;* orcid.org/0000-0003-4599-6350

Jared Sisler − *Thomas J. Watson Laboratories of Applied Physics, California Institute of Technology, Pasadena, California 91125, United States;* orcid.org/0000-0002-0660-7909

Complete contact information is available at: https://pubs.acs.org/10.1021/acsphotonics.6c00577

Author Contributions

S.I. performed the device fabrication, optical measurements, numerical simulations, and data analysis. S.U. contributed to the sample fabrication, the design of the optical measurement setup, proposed the overall concept, and led the manuscript preparation. R.S. contributed to the conceptual development of the study, device design, and simulation strategy, and provided critical input during the revision of the manuscript. J.S. assisted with the device fabrication. H.A.A. supervised the overall project. All authors discussed the results and approved the final manuscript. S.I., S.U., and R.S. contributed equally to this work.

Notes

The authors declare no competing financial interest.

■ ACKNOWLEDGMENTS

R.S., J.S., and H.A.A. gratefully acknowledge support from Hamamatsu Photonics. We acknowledge the fruitful discussions with Dr. Prachi Thureja, Dr. Martin Thomaschewski, Morgan Foley, and Juyoung (David) Kim.

■ REFERENCES

(1) Arbabi, A.; Faraon, A. Advances in Optical Metalenses. *Nat. Photonics* **2023**, *17* (1), 16−25.

(2) Wang, S.; Wu, P. C.; Su, V.-C.; Lai, Y.-C.; Chen, M.-K.; Kuo, H. Y.; Chen, B. H.; Chen, Y. H.; Huang, T.-T.; Wang, J.-H.; Lin, R.-M.; Kuan, C.-H.; Li, T.; Wang, Z.; Zhu, S.; Tsai, D. P. A Broadband Achromatic Metalens in the Visible. *Nat. Nanotechnol.* **2018**, *13* (3), 227−232.

(3) Wang, Y.; Chen, Q.; Yang, W.; Ji, Z.; Jin, L.; Ma, X.; Song, Q.; Boltasseva, A.; Han, J.; Shalaev, V. M.; Xiao, S. High-Efficiency Broadband Achromatic Metalens for near-IR Biological Imaging Window. *Nat. Commun.* **2021**, *12* (1), 5560.

(4) Chen, W. T.; Zhu, A. Y.; Sanjeev, V.; Khorasaninejad, M.; Shi, Z.; Lee, E.; Capasso, F. A Broadband Achromatic Metalens for Focusing and Imaging in the Visible. *Nat. Nanotechnol.* **2018**, *13* (3), 220−226.

(5) Khorasaninejad, M.; Chen, W. T.; Devlin, R. C.; Oh, J.; Zhu, A. Y.; Capasso, F. Metalenses at Visible Wavelengths: Diffraction-

Downloaded from pubs.acs.org/apchd5/article-pdf/13/3742/6529140/acsphotonics.6c00577.pdf by CALIFORNIA INST OF TECHNOLOGY, Ruzan Sokhoyan on 27 August 2026

Limited Focusing and Subwavelength Resolution Imaging. *Science* **2016**, *352* (6290), 1190−1194.
(6) Huang, L.; Zhang, S.; Zentgraf, T. Metasurface Holography: From Fundamentals to Applications. *Nanophotonics* **2018**, *7* (6), 1169−1190.
(7) Ni, X.; Kildishev, A. V.; Shalaev, V. M. Metasurface Holograms for Visible Light. *Nat. Commun.* **2013**, *4* (1), 2807.
(8) Zheng, G.; Mühlenbernd, H.; Kenney, M.; Li, G.; Zentgraf, T.; Zhang, S. Metasurface Holograms Reaching 80% Efficiency. *Nat. Nanotechnol.* **2015**, *10* (4), 308−312.
(9) Huang, Y.-W.; Chen, W. T.; Tsai, W.-Y.; Wu, P. C.; Wang, C.-M.; Sun, G.; Tsai, D. P. Aluminum Plasmonic Multicolor Meta-Hologram. *Nano Lett.* **2015**, *15* (5), 3122−3127.
(10) Yue, F.; Wen, D.; Xin, J.; Gerardot, B. D.; Li, J.; Chen, X. Vector Vortex Beam Generation with a Single Plasmonic Metasurface. *ACS Photonics* **2016**, *3* (9), 1558−1563.
(11) Thureja, P.; Sokhoyan, R.; Hail, C. U.; Sisler, J.; Foley, M.; Grajower, M. Y.; Atwater, H. A. Toward a Universal Metasurface for Optical Imaging, Communication, and Computation. *Nanophotonics* **2022**, *11* (17), 3745−3768.
(12) Berini, P. Optical Beam Steering Using Tunable Metasurfaces. *ACS Photonics* **2022**, *9* (7), 2204−2218.
(13) Mphuthi, N.; Gailele, L.; Litvin, I.; Dudley, A.; Botha, R.; Forbes, A. Free-Space Optical Communication Link with Shape-Invariant Orbital Angular Momentum Bessel Beams. *Appl. Opt.* **2019**, *58* (16), 4258−4264.
(14) Howes, A.; Zhu, Z.; Curie, D.; Avila, J. R.; Wheeler, V. D.; Haglund, R. F.; Valentine, J. G. Optical Limiting Based on Huygens' Metasurfaces. *Nano Lett.* **2020**, *20* (6), 4638−4644.
(15) Park, J.; Kang, J.-H.; Liu, X.; Brongersma, M. L. Electrically Tunable Epsilon-near-Zero (ENZ) Metafilm Absorbers. *Sci. Rep.* **2015**, *5* (1), 15754.
(16) Huang, Y.-W.; Lee, H. W. H.; Sokhoyan, R.; Pala, R. A.; Thyagarajan, K.; Han, S.; Tsai, D. P.; Atwater, H. A. Gate-Tunable Conducting Oxide Metasurfaces. *Nano Lett.* **2016**, *16* (9), 5319−5325.
(17) Kafaie Shirmanesh, G.; Sokhoyan, R.; Pala, R. A.; Atwater, H. A. Dual-Gated Active Metasurface at 1550 Nm with Wide (>300°) Phase Tunability. *Nano Lett.* **2018**, *18* (5), 2957−2963.
(18) Shirmanesh, G. K.; Sokhoyan, R.; Wu, P. C.; Atwater, H. A. Electro-Optically Tunable Multifunctional Metasurfaces. *ACS Nano* **2020**, *14* (6), 6912−6920.
(19) Park, J.; Jeong, B. G.; Kim, S. I.; Lee, D.; Kim, J.; Shin, C.; Lee, C. B.; Otsuka, T.; Kyoung, J.; Kim, S.; Yang, K.-Y.; Park, Y.-Y.; Lee, J.; Hwang, I.; Jang, J.; Song, S. H.; Brongersma, M. L.; Ha, K.; Hwang, S.-W.; Choo, H.; Choi, B. L. All-Solid-State Spatial Light Modulator with Independent Phase and Amplitude Control for Three-Dimensional LiDAR Applications. *Nat. Nanotechnol.* **2021**, *16* (1), 69−76.
(20) Wu, P. C.; Sokhoyan, R.; Shirmanesh, G. K.; Cheng, W.-H.; Atwater, H. A. Near-infrared Active Metasurface for Dynamic Polarization Conversion. *Adv. Opt. Mater.* **2021**, *9* (16), 2100230.
(21) Sisler, J.; Thureja, P.; Grajower, M. Y.; Sokhoyan, R.; Huang, I.; Atwater, H. A. Electrically Tunable Space-Time Metasurfaces at Optical Frequencies. *Nat. Nanotechnol.* **2024**, *19* (10), 1491−1498.
(22) Hsu, W.-C.; Chang, C.-H.; Hong, Y.-H.; Kuo, H.-C.; Huang, Y.-W. Metasurface- and PCSEL-Based Structured Light for Monocular Depth Perception and Facial Recognition. *Nano Lett.* **2024**, *24* (5), 1808−1815.
(23) Xie, Y.-Y.; Ni, P.-N.; Wang, Q.-H.; Kan, Q.; Briere, G.; Chen, P.-P.; Zhao, Z.-Z.; Delga, A.; Ren, H.-R.; Chen, H.-D.; Xu, C.; Genevet, P. Metasurface-Integrated Vertical Cavity Surface-Emitting Lasers for Programmable Directional Lasing Emissions. *Nat. Nanotechnol.* **2020**, *15* (2), 125−130.
(24) Zhuo, S.; Li, Y.; Zhao, A.; Li, Y.-R.; Yao, S.; Zhang, M.; Feng, T.; Li, Z. Dynamic Transmissive Metasurface for Broadband Phase-only Modulation Based on Phase-change Materials. *Laser Photon. Rev.* **2023**, *17* (1), 2200403.
(25) Komar, A.; Paniagua-Domínguez, R.; Miroshnichenko, A.; Yu, Y. F.; Kivshar, Y. S.; Kuznetsov, A. I.; Neshev, D. Dynamic Beam Switching by Liquid Crystal Tunable Dielectric Metasurfaces. *ACS Photonics* **2018**, *5* (5), 1742−1748.
(26) Li, S.-Q.; Xu, X.; Maruthiyodan Veetil, R.; Valuckas, V.; Paniagua-Domínguez, R.; Kuznetsov, A. I. Phase-Only Transmissive Spatial Light Modulator Based on Tunable Dielectric Metasurface. *Science* **2019**, *364* (6445), 1087−1090.
(27) Sisler, J.; Hail, C. U.; Davidson, Z. S.; Fehr, A. M. K.; Gao, J.; Sokhoyan, R.; Elhadj, S.; Atwater, H. A.An Optically Addressable Transmissive Liquid Crystal Metasurface Spatial Light Modulator-*arXiv: 2603.20574***2026**
(28) Karst, J.; Floess, M.; Ubl, M.; Dingler, C.; Malacrida, C.; Steinle, T.; Ludwigs, S.; Hentschel, M.; Giessen, H. Electrically Switchable Metallic Polymer Nanoantennas. *Science* **2021**, *374* (6567), 612−616.
(29) Arbabi, E.; Arbabi, A.; Kamali, S. M.; Horie, Y.; Faraji-Dana, M.; Faraon, A. MEMS-Tunable Dielectric Metasurface Lens. *Nat. Commun.* **2018**, *9* (1), 812.
(30) Han, Z.; Colburn, S.; Majumdar, A.; Böhringer, K. F. MEMS-Actuated Metasurface Alvarez Lens. *Microsyst. Nanoeng.* **2020**, *6* (1), 79.
(31) Soma, G.; Ariu, K.; Karakida, S.; Tsubai, Y.; Tanemura, T. Subvolt High-Speed Free-Space Modulator with Electro-Optic Metasurface. *Nat. Nanotechnol.* **2025**, *20* (11), 1625−1632.
(32) Benea-Chelmus, I.-C.; Meretska, M. L.; Elder, D. L.; Tamagnone, M.; Dalton, L. R.; Capasso, F. Electro-Optic Spatial Light Modulator from an Engineered Organic Layer. *Nat. Commun.* **2021**, *12* (1), 5928.
(33) Weigand, H.; Vogler-Neuling, V. V.; Escalé, M. R.; Pohl, D.; Richter, F. U.; Karvounis, A.; Timpu, F.; Grange, R. Enhanced Electro-Optic Modulation in Resonant Metasurfaces of Lithium Niobate. *ACS Photonics* **2021**, *8* (10), 3004−3009.
(34) Dagli, S.; Shim, J.; Carr Delgado, H.; Balch, H. B.; Abdollahramezani, S.; Chen, C.-Y.; Dolia, V.; Klopfer, E.; Dixon, J.; Hu, J.; Ogunlade, B.; Song, J.-H.; Brongersma, M. L.; Barton, D.; Dionne, J. A. GHz-Speed Wavefront Shaping Metasurface Modulators Enabled by Resonant Electro-Optic Nanoantennas. *Adv. Mater.* **2025**, *37* (40), No. e06790.
(35) Thomaschewski, M.; Sokhoyan, R.; Schneider, E.; Atwater, H. A.Picometer-Scale Spatial Symmetry Breaking in Active Transmissive Metasurfaces*arXiv: 2604.15185***2026**
(36) Howes, A.; Wang, W.; Kravchenko, I.; Valentine, J. Dynamic transmission control based on all-dielectric Huygens metasurfaces. *Optica* **2018**, *5* (7), 787−792.
(37) Thomaschewski, M.; Dong, C.; Gui, Y.; Wang, H.; Dalir, H.; Sorger, V. J. Free-Space Indium Tin Oxide Electro-Optic Transmission Modulator. *ACS Photonics* **2025**, *12* (1), 202−206.
(38) Lee, Y.; Yun, J.; Kim, S.-J.; Seo, M.; In, S.; Jeong, H.-D.; Lee, S.-Y.; Park, N.; Chung, T. D.; Lee, B. High-speed Transmission Control in Gate-tunable Metasurfaces Using Hybrid Plasmonic Waveguide Mode. *Adv. Opt. Mater.* **2020**, *8* (22), 2001256.
(39) Forouzmand, A.; Salary, M. M.; Kafaie Shirmanesh, G.; Sokhoyan, R.; Atwater, H. A.; Mosallaei, H. Tunable All-Dielectric Metasurface for Phase Modulation of the Reflected and Transmitted Light via Permittivity Tuning of Indium Tin Oxide. *Nanophotonics* **2018**, *8* (3), 415−427.
(40) Uenoyama, S.; Tanaka, K.; Fujiwara, H.; Watanabe, A.; Ono, A. Experimental Demonstration of Improvement in Near-Infrared Photodetection Efficiency by Plasmonic Diffraction. *ACS Appl. Electron. Mater.* **2024**, *6*, 7046.
(41) Kim, J.; Sokhoyan, R.; Yi, M.; Han, S.; Atwater, H. A.; Jang, M. S. Overcoming Barriers to Dynamic Phase-Only Modulation in Transmissive Metasurfaces via Diffraction Control. *ACS Nano* **2026**, *20* (8), 6622−6631.
(42) Sokhoyan, R.; Thureja, P.; Sisler, J.; Grajower, M.; Shayegan, K.; Feigenbaum, E.; Elhadj, S.; Atwater, H. A. Electrically Tunable Conducting Oxide Metasurfaces for High Power Applications. *Nanophotonics* **2023**, *12* (2), 239−253.

Downloaded from pubs.acs.org/apchd5/article-pdf/13/13742/6529409/acsphotonics.6c00577.pdf by CALIFORNIA INST OF TECHNOLOGY, Ruzan Sokhoyan on 27 August 2026

https://doi.org/10.1021/acsphotonics.6c00577
ACS Photonics 2026, 13, 3742−3749